

## COLD ACCRETION IN EARLY GALAXY FORMATION AND ITS Ly $\alpha$ SIGNATURES

HIDENOBU YAJIMA<sup>1,2</sup>, YUEXING LI<sup>3,4</sup>, QIRONG ZHU<sup>3,4</sup>, TOM ABEL<sup>5</sup>

<sup>1</sup> Department of Earth & Space Science, Graduate School of Science, Osaka University, 1-1 Machikaneyama, Toyonaka, Osaka 560-0043, Japan

<sup>2</sup> Institute for Astronomy, University of Edinburgh, Royal Observatory, Edinburgh, EH9 3HJ, UK

<sup>3</sup> Department of Astronomy & Astrophysics, The Pennsylvania State University, 525 Davey Lab, University Park, PA 16802, USA

<sup>4</sup> Institute for Gravitation and the Cosmos, The Pennsylvania State University, University Park, PA 16802, USA and

<sup>5</sup> Kavli Institute for Particle Astrophysics and Cosmology, SLAC National Accelerator Laboratory, Stanford University, 2575 Sand Hill Road, Menlo Park, CA 94025, USA

*Draft version February 7, 2022*

### ABSTRACT

The Ly $\alpha$  emission has played an important role in detecting high-redshift galaxies, including recently distant ones at redshift  $z > 7$ . It may also contain important information on the origin of these galaxies. Here, we investigate the formation of a typical  $L^*$  galaxy and its observational signatures at the earliest stage, by combining a cosmological hydrodynamic simulation with three-dimensional radiative transfer calculations using the newly improved ART<sup>2</sup> code. Our cosmological simulation uses the Aquila initial condition which zooms in onto a Milky Way-like halo with high resolutions, and our radiative transfer couples multi-wavelength continuum, Ly $\alpha$  line, and ionization of hydrogen. We find that the modeled galaxy starts to form at redshift  $z \sim 24$  through efficient accretion of cold gas, which produces a strong Ly $\alpha$  line with a luminosity of  $L_{\text{Ly}\alpha} \sim 10^{42}$  erg s<sup>-1</sup> as early as  $z \sim 14$ . The Ly $\alpha$  emission appears to trace the cold, dense gas. The lines exhibit asymmetric, single-peak profiles, and are shifted to the blue wing, a characteristic feature of gas inflow. Moreover, the contribution to the total Ly $\alpha$  luminosity by excitation cooling increases with redshift, and it becomes dominant at  $z \gtrsim 6$ . We predict that  $L^*$  galaxies such as the modeled one may be detected at  $z \lesssim 8$  by JWST and ALMA with a reasonable integration time. Beyond redshift 12, however, only Ly $\alpha$  line may be observable by spectroscopic surveys. Our results suggest that Ly $\alpha$  line is one of the most powerful tools to detect the first generation of galaxies, and to decipher their formation mechanism.

*Subject headings:* galaxies: formation – galaxies: evolution – galaxies: high-redshift – radiative transfer  
– line: profiles – hydrodynamics – cosmology: computation

### 1. INTRODUCTION

The quest for the first galaxies formed at the cosmic dawn is a major frontier in both observational and theoretical cosmology (Bromm & Yoshida 2011). Over the past few years, significant progress has been made in detecting galaxies at redshift  $z \gtrsim 6$ , using either broad-band colors (e.g., Bouwens et al. 2004; Bouwens & Illingworth 2006; Bouwens et al. 2010, 2011), or narrow-band Ly $\alpha$  emission line (e.g., Malhotra & Rhoads 2004; Iye et al. 2006; Stark et al. 2007; Hu et al. 2010; Lehnert et al. 2010; Vanzella et al. 2011; Stark et al. 2011; Ono et al. 2012; Kashikawa et al. 2011; Shibuya et al. 2012; Finkelstein et al. 2013). In particular, the Ly $\alpha$  line has played an important role in identifying and confirming distant galaxies, the so-called Ly $\alpha$  emitters (LAEs), including currently the record holder at  $z = 8.6$  (Lehnert et al. 2010). These remarkable observations indicate that galaxies formed less than a few hundred million years after the Big Bang.

Despite the rapidly increasing number of detections, the origin and nature of these distant galaxies, however, remain open questions (Bromm et al. 2009). Recently, a number of state-of-the-art simulations have started to address this issue (e.g., Wise & Abel 2007; Wise et al. 2008; Wise & Abel 2008; Greif et al. 2010; Wise et al. 2012; Jeon et al. 2012). These studies focused on a halo

in a small volume (1 Mpc) with high resolutions, and suggested that the formation of the first galaxies is closely tied to the formation of the first stars (so-called Pop III stars) and the feedback from them, and that these galaxies likely consist of second- or third generation of stars formed from enriched gas, similar to the present-day stars.

In this work, we explore the physical conditions of early galaxy formation on a larger scale. In particular, we focus on the gas properties and the Ly $\alpha$  emission from it. Recent simulations have revealed that a large amount of gas penetrate deep inside dark matter halos as cold, filamentary streams (Katz et al. 2003; Birnboim & Dekel 2003; Kereš et al. 2005, 2009; Dekel & Birnboim 2006; Ocvirk et al. 2008; Brooks et al. 2009; Dekel et al. 2009), and Dekel et al. (2009) showed that massive galaxies at  $z = 2 - 3$  can actively form stars from inflow of cold gas. More recently, Di Matteo et al. (2011) suggested that massive galaxies at  $z \gtrsim 6$  can grow by cold accretion and evolve with black holes. Such streams of cold gas may produce a large number of Ly $\alpha$  photons via excitation cooling process, and give rise to the Ly $\alpha$  emission detected in the early galaxies (Dijkstra & Loeb 2009; Faucher-Giguère et al. 2010; Latif et al. 2011; Yajima et al. 2012a,b).

We combine a multi-scale cosmological hydrodynamic simulation with multi-wavelength radiative transfer (RT) calculations. The simulation uses the Aquila initial condition and follows the formation and evolution of

a Milky Way-size galaxy (Wadepuhl & Springel 2011; Scannapieco et al. 2012). It covers a large dynamical range from a  $100 h^{-1}\text{Mpc}$  box down to a  $\sim 5 h^{-3}\text{Mpc}$  zoom-in region, which is ideal to study the gas inflow on a large scale. The RT calculations uses the three-dimensional Monte Carlo RT code ART<sup>2</sup> by Li et al. (2008); Yajima et al. (2012a). The ART<sup>2</sup> code couples multi-wavelength continuum, Ly $\alpha$  line, and ionization of hydrogen, which is critical to study the Ly $\alpha$  and multi-band properties of the early galaxies.

The paper is organized as follows. We describe our cosmological simulation in §2, and the RT calculations in §3. In §4, we present the results, which include the Ly $\alpha$  properties, and detectability by upcoming missions *James Webb Space Telescope* (JWST) and *Atacama Large Millimeter Array* (ALMA). We discuss the implications and limitations of our model in §5, and summarize in §6.

## 2. MODEL & METHODOLOGY

We carry out a cosmological simulation with the Aquila initial condition which can reproduce a Milky Way-like galaxy at  $z = 0$  (Springel et al. 2008; Scannapieco et al. 2012). The whole simulation box is  $100 h^{-1}\text{Mpc}$  on each side with a zoom-in region of a size of  $5 \times 5 \times 5 h^{-3}\text{Mpc}^3$ . The spatial resolution in the zoom-in region is  $\sim 250 h^{-1}\text{pc}$  and the mass resolution is  $1.8 \times 10^6 h^{-1}M_{\odot}$  for dark matter particles,  $3 \times 10^5 h^{-1}M_{\odot}$  for gas, and  $1.5 \times 10^5 h^{-1}M_{\odot}$  for star particles. The cosmological parameters used in the simulation are  $\Omega_m = 0.25$ ,  $\Omega_{\Lambda} = 0.75$ ,  $\sigma_8 = 0.9$  and  $h = 0.73$ , consistent with the five-year results of the WMAP (Komatsu et al. 2009). The simulation was performed using the N-body/Smoothed Particle Hydrodynamics (SPH) code GADGET-3 (Springel et al. 2001; Springel 2005). The specifics of the simulation were described in Zhu et al. (2012), and we refer the readers to that paper for more details.

In this work, we use the 3D Monte Carlo RT code, All-wavelength Radiative Transfer with Adaptive Refinement Tree (ART<sup>2</sup>) to study the multi-wavelength properties of the model galaxies. The ART<sup>2</sup> code includes continuum photons from X-ray to radio, Ly $\alpha$  line, and ionization structure in the adaptive refinement grids. The detailed prescriptions of the code were presented in Li et al. (2008) and Yajima et al. (2012a). The Ly $\alpha$  emission comes from the recombination and de-excitation process,

$$\epsilon_{\text{Ly}\alpha} = f_{\alpha} \alpha_{\text{B}} h \nu_{\alpha} n_{\text{e}} n_{\text{HII}} + C_{\text{Ly}\alpha} n_{\text{e}} n_{\text{HI}}, \quad (1)$$

where  $\alpha_{\text{B}}$  is the case B recombination coefficient, and  $f_{\alpha}$  is the average number of Ly $\alpha$  photons produced per case B recombination. The  $\alpha_{\text{B}}$  derived in Hui & Gnedin (1997) is used. Due to the small dependence of  $f_{\alpha}$  to temperature, we assume  $f_{\alpha} = 0.68$  at everywhere (Osterbrock & Ferland 2006). The  $C_{\text{Ly}\alpha}$  is the collisional excitation coefficient,  $C_{\text{Ly}\alpha} = 3.7 \times 10^{-17} \exp(-h\nu_{\alpha}/kT) T^{-1/2} \text{erg s}^{-1} \text{cm}^3$  (Osterbrock & Ferland 2006). The Ly $\alpha$  emissivity and opacity highly depend on the ionization structure in the galaxies. We at first calculate the ionization structure due to internal stellar sources, then simulate the Ly $\alpha$  RT. We cast  $N_{\text{ph}} = 10^5$  photon packets for each ionizing, Ly $\alpha$ , and non-ionizing components, which showed good convergence (Yajima et al. 2012a,b). In addition, inter-

stellar dust is included to consider the dust extinction of Ly $\alpha$  and continuum photons, and to simulate the dust thermal emission (see also Yajima et al. 2012a). The intrinsic spectral energy distributions (SEDs) of stars are calculated by GALAXEV (Bruzual & Charlot 2003) with the assumption of Salpeter IMF. For the SED of AGNs, the broken power law is used (Li et al. 2008). For the intrinsic SEDs, we do not include Ly $\alpha$  line as nebula emission. This is because we here calculate the radiative transfer of ionizing photons and ionization structure. Some fraction of ionizing photons are absorbed in situ, and converted to Ly $\alpha$  photons via the recombination process. Therefore, the nebula emission at Ly $\alpha$  line is included in the post-processing calculations.

## 3. RESULTS

In our previous work, we have presented the formation history of a MW galaxy in Zhu et al. (2010), and have applied ART<sup>2</sup> to the Aquila simulation to study the multi-band properties of the MW progenitors (Yajima et al. 2012a), and the escape of Ly $\alpha$  and continuum photons (Yajima et al. 2012b). In this paper, we focus on the earliest evolutionary stage of the MW and the Ly $\alpha$  properties from  $z \sim 6 - 14$ .

### 3.1. The Accretion of Cold Gas

The modeled MW galaxy starts to form at  $z \sim 24$ . Figure 1 shows the distribution of gas density, gas temperature, and stellar density of the MW main progenitor from redshift  $z \sim 14$  to  $z \sim 6$ . The gas follows the distribution of dark matter and exhibits filamentary structures. At  $z \gtrsim 6$ , the gas is predominantly cold, with a mean temperature of  $\sim 10^4$  K. Stars form out of such cold gas, so they also distribute along the filaments.

The star formation at  $z \gtrsim 6$  is fueled by efficient accretion of cold gas, as demonstrated in Figure 2. The gas accretion rate is defined as the inflow rate of gas within the virial radius of the modeled galaxy. It peaks around  $10^4$  K in all cases. At a later time, feedback from both stars and accreting BHs heats up the gas. Also, the gas can be heated by gravitational shocks during the infall. Therefore the accretion includes hot gas as well. The inflow gas falls along the filaments toward the intersection, the highest density peak where the first galaxy in the simulated volume forms.

Figure 3 shows the star formation history of the MW. The star formation rate (SFR) increases steadily from  $\sim 3 \times 10^{-3} M_{\odot} \text{yr}^{-1}$  at  $z \sim 24$  to  $\sim 15 M_{\odot} \text{yr}^{-1}$  at  $z \sim 8.5$ , and it peaks at  $\sim 62 M_{\odot} \text{yr}^{-1}$  at  $z = 5.2$ , due to the merging processes of gas-rich galaxies. The galaxy mass increases rapidly during this cold accretion phase. By  $z \sim 8.5$ , it reaches a total mass of  $\sim 5.6 \times 10^{10} M_{\odot}$ , and a stellar mass of  $\sim 6 \times 10^9 M_{\odot}$ .

### 3.2. The Ly $\alpha$ Properties

The Ly $\alpha$  emission traces the gas distribution, as shown in Figure 4. The surface brightness rises above  $10^{-20} \text{erg s}^{-1} \text{cm}^{-2} \text{arcsec}^{-2}$  at  $z \lesssim 14$ . At high redshift  $z \gtrsim 10$ , the galaxy is small, and the Ly $\alpha$  emission is faint and confined to the central high-density region. The Ly $\alpha$  emission increases with the mass and size of the galaxy, and it becomes stronger and more extended and irregular due to mergers and gas infall along the filaments of the main halo.

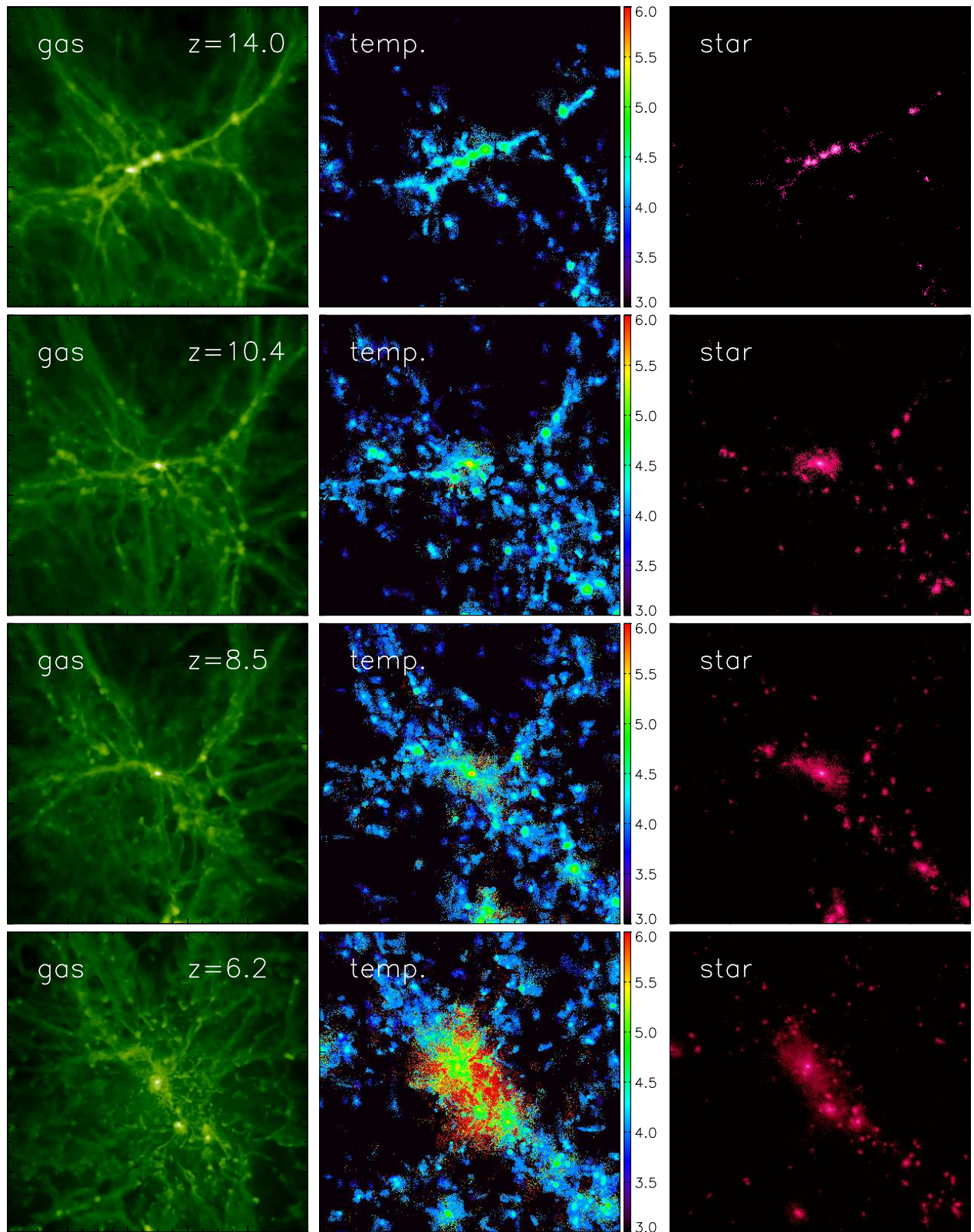


**Figure 1.** The distribution of gas density (left column), gas temperature (middle column), and stellar density (right column), of the MW galaxy at  $z \sim 14, 10.4, 8.5,$  and  $6.2,$  respectively. The box size is 1 Mpc in comoving scale. The temperature of the gas is in Kelvin in log scale, as indicated in the color bar.

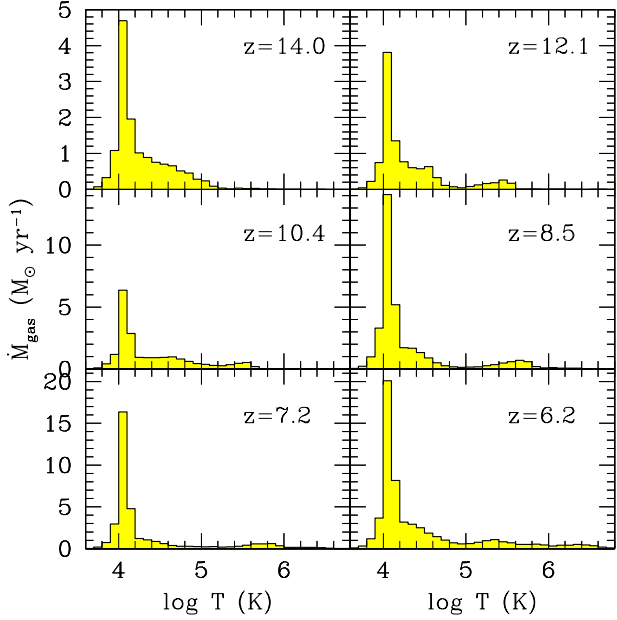


**Figure 2.** The gas accretion rate by the MW galaxy as a function of gas temperature at different redshift.

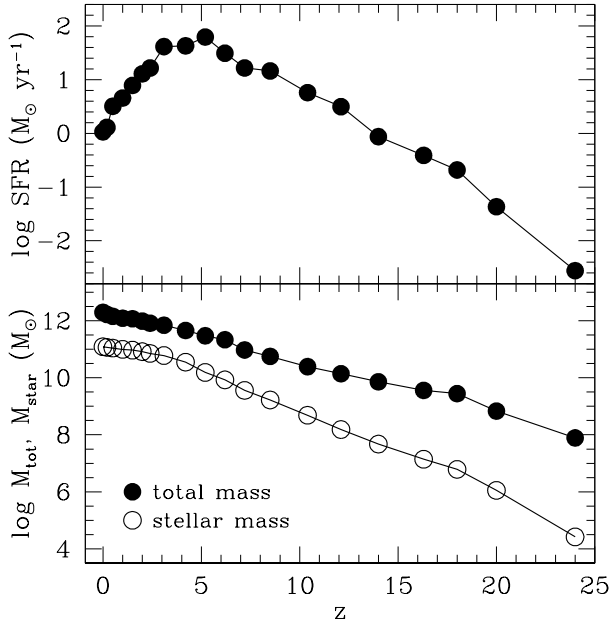


**Figure 3.** The growth history of the MW galaxy illustrated by the star formation rate (top panel), and by the accumulated mass (bottom panel), in which filled circle represents the total mass, while the open circle represents the stellar mass.

Figure 5 shows the Ly $\alpha$  properties of the MW galaxy at from  $z \sim 14$  to  $z \sim 6$ , including the emergent Ly $\alpha$  luminosity ( $L_{\text{Ly}\alpha}$ ), equivalent width of Ly $\alpha$  line in rest frame, and photon escape fraction of Ly $\alpha$  and UV continuum (1300 - 1600 Å). For comparison with the star formation activity, the SFR of the galaxy at corresponding redshift is also shown.

During this early growth phase, the SFR of the galaxy increases from  $\sim 1 M_{\odot} \text{ yr}^{-1}$  at  $z \sim 14.0$  to  $\sim 31 M_{\odot} \text{ yr}^{-1}$

at  $z \sim 6$ , owing to abundant supply of cold gas from infall and merging of gas-rich mini halos. The resulting emergent Ly $\alpha$  luminosity shows a similar trend, increasing from  $\sim 1.6 \times 10^{42} \text{ erg s}^{-1}$  at  $z \sim 14.0$  to  $\sim 5.5 \times 10^{42} \text{ erg s}^{-1}$  at  $z \sim 6$ . If we consider only the recombination process with the assumption of  $L_{\text{Ly}\alpha}/L_{\text{H}\alpha} = 8.7$  (in which the H $\alpha$  is a tracer of star formation), the intrinsic Ly $\alpha$  luminosity should be linearly proportional to SFR,  $L_{\text{Ly}\alpha} (\text{erg s}^{-1}) = 1.1 \times 10^{42} \times \text{SFR} (M_{\odot} \text{ yr}^{-1})$  (Kennicutt 1998). However, the evolution of  $L_{\text{Ly}\alpha}$  in Figure 5 differs from the SFR history. This is due to the contribution from excitation cooling to the Ly $\alpha$  emission as we will discuss later, and dust absorption of the Ly $\alpha$  photons. In particular, at  $z \gtrsim 10$ , the  $L_{\text{Ly}\alpha}$  increases with redshift, in opposite direction from the SFR, as a result of high collisional excitation and high  $f_{\text{esc}}$ .

The lower-left panel of Figure 5 shows the photon escape fraction of Ly $\alpha$ ,  $f_{\text{esc}}^{\text{Ly}\alpha}$ , and the UV continuum  $f_{\text{esc}}^{\text{UV}}$ , where  $f_{\text{esc}}^{\text{UV}}$  is calculated at  $\lambda_{\text{rest}} = 1300 - 1600 \text{ \AA}$ . The  $f_{\text{esc}}^{\text{Ly}\alpha}$  of the modeled galaxy falls in the range of 0.49 - 0.81, and it increases with redshift. In our model, the dust is produced by type-II supernovae (Li et al. 2008). The dust amount increases as star formation rises from  $z \sim 14$  to  $z \sim 6$ , and hence it efficiently absorbs the Ly $\alpha$  and UV continuum photons, resulting decreasing escape fraction. However even at  $z = 8.5$ , about 40% of Ly $\alpha$  photons are absorbed by dust. This is due to the fact that, in the early phase, galaxies are gas rich and compact, the gas and dust are highly concentrated in the galaxies, resulting in effective absorption of the Ly $\alpha$  and UV photons by the dust.

The resulting Ly $\alpha$  equivalent width (EW) is shown in the lower-right panel of Figure 5. The EW is estimated from the Ly $\alpha$  flux divided by the UV flux density at  $\lambda = 1300 - 1600 \text{ \AA}$ . The modeled galaxy has  $\text{EW} \gtrsim 20 \text{ \AA}$  at these redshifts, and is therefore classified as a Ly $\alpha$  emitter (LAE) (e.g., Gronwall et al. 2007). The EW increases with redshift, from  $\sim 93 \text{ \AA}$  at  $z \sim 6$  to  $\sim 2300 \text{ \AA}$  at  $z \sim 14.0$ . Such trend is similar to that reported in recent observations which showed that galaxies at higher redshift have higher EWs than their lower-redshift counterparts (e.g., Gronwall et al. 2007; Ouchi et al. 2008). This is because the contribution from excitation Ly $\alpha$  cooling becomes large with increasing redshift, as shown in Figure 6 in the next section, which boosts the EW significantly (Yajima et al. 2012a,b).

The currently most distant LAE at  $z = 7.5$ , z8.GND.5296, has a Ly $\alpha$  luminosity of  $\sim 1.8 \times 10^{42} \text{ erg s}^{-1}$  (Finkelstein et al. 2013). Our model shows the similar Ly $\alpha$  luminosity at the redshift, and hence may be reproducing the observed LAE. However, there are additional uncertainties which may reduce the Ly $\alpha$  flux of our calculation as we explain at the below and Section 3.4.

Next generation telescopes will have very high-angular resolution, for example, that of JWST will get to  $\lesssim 0.1''$ . Some extended fainter parts as seen in Figure 4 can be lost in observation with such the resolution. As a result, observed Ly $\alpha$  flux is likely to be lower than that galaxies are actually emitting. In practice, for Figure 4, if we count up only fluxes of pixels brighter than  $10^{-18} \text{ erg s}^{-1} \text{ cm}^{-2} \text{ arcsec}^{-2}$ , which is the detection threshold of recent observation of extended Ly $\alpha$  source

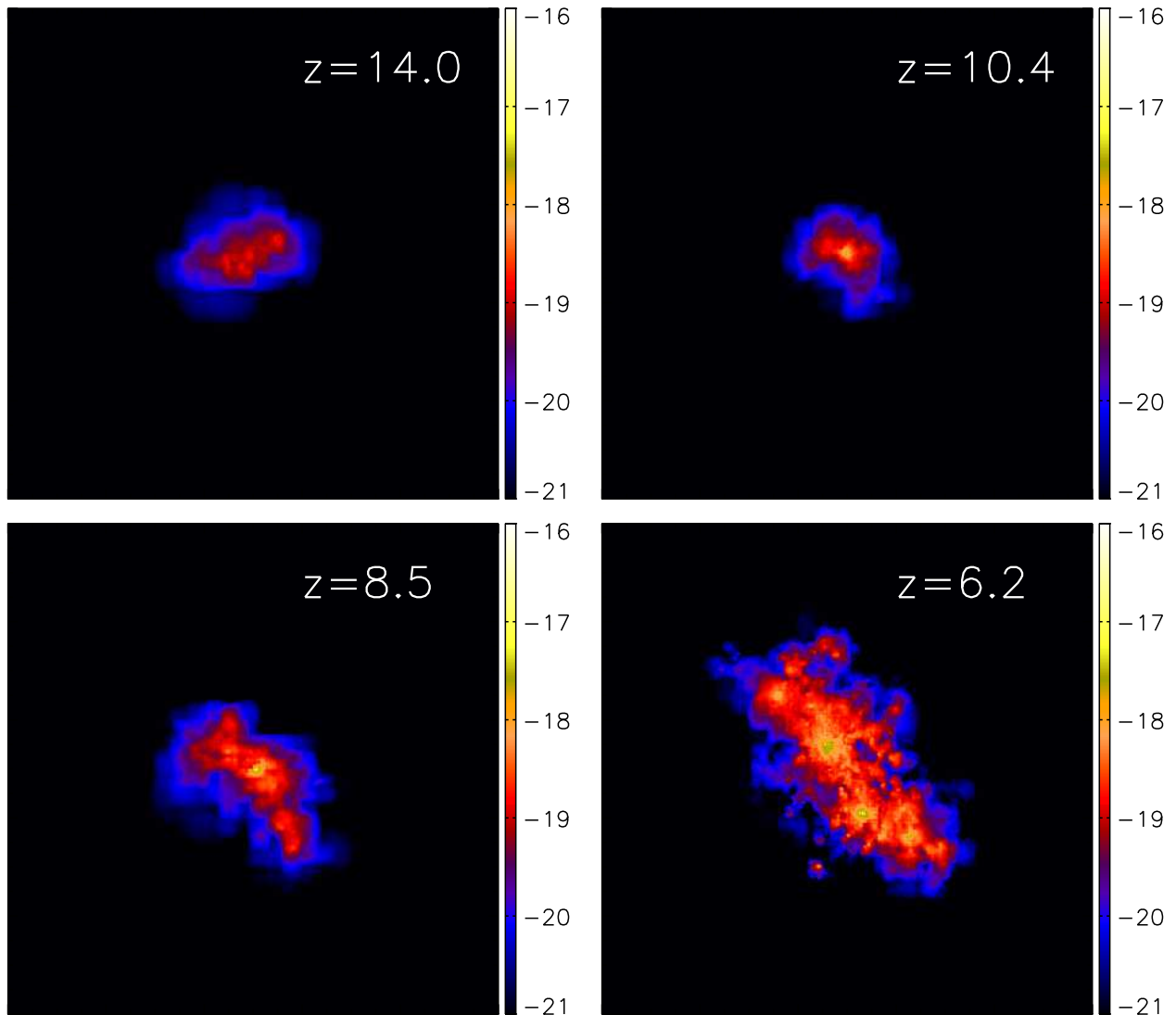


**Figure 4.** The evolution of the Ly $\alpha$  surface brightness of the MW galaxy with redshift, at  $z \sim 14, 10.4, 8.5,$  and  $6.2,$  respectively. The box size is 1 Mpc in comoving scale. The color indicates the Ly $\alpha$  surface brightness in log scale in units of  $\text{erg s}^{-1} \text{cm}^{-2} \text{arcsec}^{-2}.$

with a narrow-band filter (e.g., Matsuda et al. 2012), the Ly $\alpha$  fluxes are reduced by factor  $\sim 5.7$  at  $z = 6.2$  and  $\sim 61.0$  at  $z = 12.1$ . Open triangles and squares in the Figure 5 show the Ly $\alpha$  properties by considering the detection thresholds of the surface brightness with  $10^{-18}$  and  $10^{-19} \text{ erg s}^{-1} \text{cm}^{-2} \text{arcsec}^{-2},$  respectively. Ly $\alpha$  luminosity and EW of our model galaxies can be significantly reduced in the mock observation with the threshold of  $10^{-18} \text{ erg s}^{-1} \text{cm}^{-2} \text{arcsec}^{-2}.$  In particular, the galaxies at  $z > 10$  become too faint to be detected in the current observation. On the other hand, if the surface brightness threshold is  $\sim 10^{-19} \text{ erg s}^{-1} \text{cm}^{-2} \text{arcsec}^{-2},$  we detect 85.9 per cent of the flux for  $z = 6.2$  and 42.5 per cent for  $z = 12.1.$  However, the narrow-band filter imaging by F164N on JWST will require very long exposure time  $\gtrsim 10^4$  hours to achieve the detection threshold for  $5 \sigma$  detection. Therefore, although galaxies have complex Ly $\alpha$  distribution reflecting gas and stellar distribution, most of them can be lost in observation. Due to the lost of faint extended parts, the high- $z$  galaxies can be faint at Ly $\alpha$  band or undetectable with current

(or future) observations, although they are intrinsically bright.

### 3.3. Contribution of Excitation Cooling to Ly $\alpha$ Emission

As mentioned in § 2, the Ly $\alpha$  emission is generally produced by the recombination of ionizing photons and the collisional excitation of hydrogen gas. In our cosmological simulation, galaxy evolution is accompanied by cold, filamentary gas streams with temperature  $T \sim 10^{4-5} \text{ K},$  which penetrate deep inside the dark matter halos (Zhu et al. in prep, Yajima et al. 2012b), which was also shown by previous theoretical works (Katz et al. 2003; Kereš et al. 2005, 2009; Birnboim & Dekel 2003; Dekel & Birnboim 2006; Ocvirk et al. 2008; Brooks et al. 2009; Dekel et al. 2009). The Ly $\alpha$  emissivity due to collisional excitation is sensitive to gas temperature, and has the peak in the efficiency at  $T \sim 10^4 \text{ K}$  (Faucher-Giguère et al. 2009). Hence, much excitation Ly $\alpha$  cooling photons can be emitted from such cold accreted gas (Dijkstra & Loeb

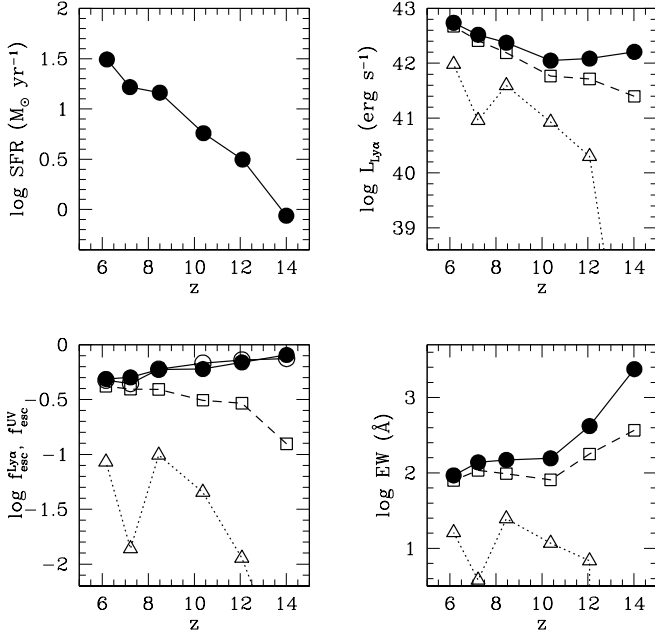


**Figure 5.** The Ly $\alpha$  properties of the modeled galaxy from  $z \sim 14$  to  $z \sim 6$ , including, in clockwise direction, star formation rate, emergent Ly $\alpha$  luminosity, equivalent width of Ly $\alpha$  line in rest frame, and photon escape fraction of Ly $\alpha$  (filled circles) and UV continuum (1300 - 1600 Å, open circles). Open triangles and squares represent the modified Ly $\alpha$  properties considering the detection thresholds of the surface brightness with  $10^{-18}$  and  $10^{-19}$  erg s $^{-1}$  cm $^{-2}$  arcsec $^{-2}$ , respectively.

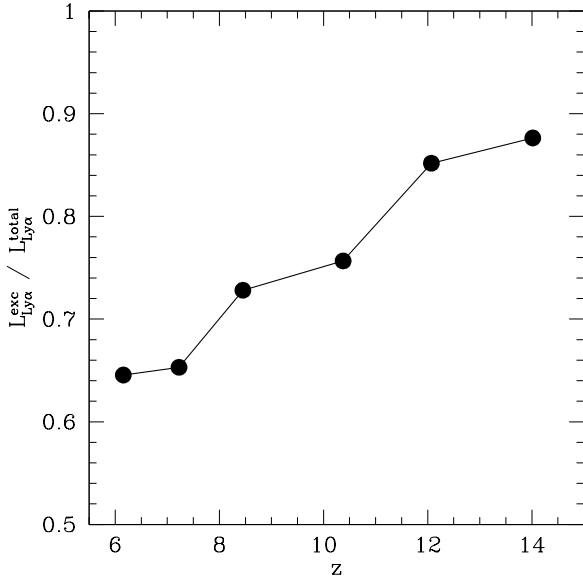


**Figure 6.** The fraction of excitation cooling Ly $\alpha$  to the total intrinsic Ly $\alpha$  luminosity as a function of redshift from  $z \sim 14$  to  $z \sim 6$ .

2009; Faucher-Giguère et al. 2009; Goerdt et al. 2010). At higher redshift, galaxies experience more merging events and accrete more cold gas efficiently, which results in stronger Ly $\alpha$  emission from excitation cooling, and higher Ly $\alpha$  EWs (Yajima et al. 2012a,b).

As shown in Figure 6, the fraction of intrinsic excitation cooling Ly $\alpha$  to the total intrinsic Ly $\alpha$  luminosity increases from  $\sim 65\%$  at  $z \sim 6$  to  $\sim 88\%$  at  $z \sim 14$ . Such extremely high excitation Ly $\alpha$  cooling produces the extremely high Ly $\alpha$  EWs seen in Figure 5.

The Ly $\alpha$  luminosity of our model, which is mainly contributed by the excitation cooling, is higher than the model at  $z = 3$  in Faucher-Giguère et al. (2010). For example, they showed  $L_{\text{Ly}\alpha} \lesssim 10^{42}$  erg s $^{-1}$  at the halo mass  $M_h \sim 10^{11} M_\odot$ . On the other hand, when our model galaxy has similar mass at  $z = 7.2$ , it shows  $L_{\text{Ly}\alpha} = 6.6 \times 10^{42}$  erg s $^{-1}$  without dust extinction. This may be due to the difference of the conversion efficiency from gravitational energy to Ly $\alpha$  cooling. Faucher-Giguère et al. (2010) used 0.3 as the conversion efficiency (see also Dijkstra & Loeb 2009). In addition, recently Rosdahl & Blaizot (2012) showed the conversion efficiency is  $\sim 0.1-0.2$  by radiative-hydrodynamics simulations. However, this conversion efficiency depends sensitively on the detailed gas structure in and around galaxies (Rosdahl & Blaizot 2012). In some situations, cold-accreted gas is disturbed by interstellar gas and heated up (Rosdahl & Blaizot 2012). In our model, galaxies are compact and high-density (Yajima et al. 2012c), hence a large fraction of accreted gas might be heated due to friction with interstellar medium. Then, since the temperature of the cold accretion gas is  $\gtrsim 10^4$  K, most of the thermal energy can be converted to Ly $\alpha$  photons (Thoul & Weinberg 1996). In addition, Ly $\alpha$  luminosity by the excitation cooling can increase with redshift, because the Ly $\alpha$  emissivity is proportional to square of gas density (Equation 1) and mean gas density of galaxies increases with redshift (e.g., Bryan & Norman 1998). In practice, Goerdt et al. (2010) showed that  $L_{\text{Ly}\alpha} = 1.88 \times 10^{42}$  erg s $^{-1}$   $(M_h/10^{12} M_\odot)^{0.8} (1+z)^{1.3}$  by their cosmological hydrodynamics simulations with a simple dust absorption model. The Ly $\alpha$  luminosities of our model galaxies are consistent with their estimation. Note that, the Ly $\alpha$  cooling rate balances heating rate and it is sensitive to temperature. The heating rate may not simply increase with redshift while the mean gas density does. If gas temperature is higher than  $\sim 10^6$  K, the thermal energy can be released by different cooling radiation, e.g., recombination, free-free emission (Thoul & Weinberg 1996). In addition, the Ly $\alpha$  luminosity by the excitation cooling in our simulations at  $z = 3$ , which is  $L_{\text{Ly}\alpha} = 1.9 \times 10^{42}$  erg s $^{-1}$  at  $M_h = 5.9 \times 10^{11} M_\odot$ , is close to that in Faucher-Giguère et al. (2010). Thus, the Ly $\alpha$  luminosity of our model at  $z > 6$  can be higher than the analytical model of Faucher-Giguère et al. (2010) at  $z = 3$  by some factors.

The current our code does not distinguish excitation and recombination Ly $\alpha$  photons in the RT calculations. However, the fraction of excitation Ly $\alpha$  cooling rate may not change significantly for mock observations with the different thresholds of surface brightness. This is because, as shown in Yajima et al. (2012b), Ly $\alpha$  photons are mostly emitted at galactic centers, and travel with

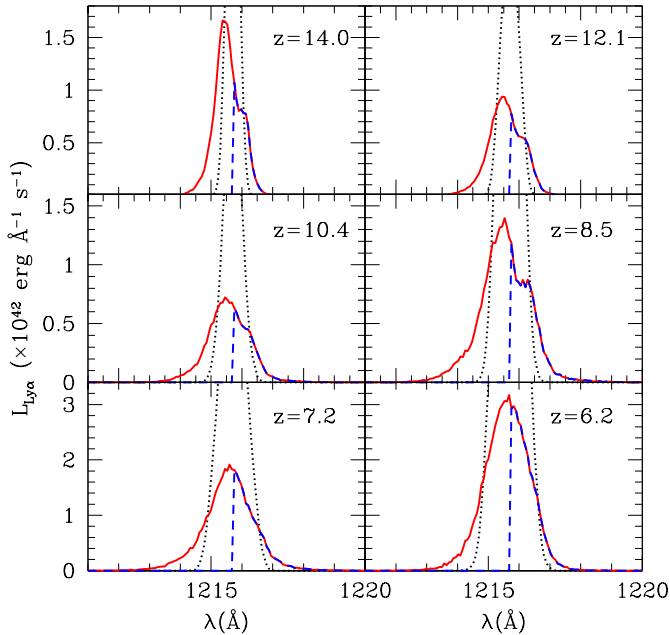


**Figure 7.** The Ly $\alpha$  line profile of the modeled galaxy at different redshifts. The black dotted- and red solid lines are the intrinsic and emergent Ly $\alpha$  profiles, respectively. The blue dash lines are the Ly $\alpha$  profiles with cutting off Ly $\alpha$  flux at  $\lambda < 1216$  Å due to IGM transmission (Laursen et al. 2011).

many scatterings in inter-stellar medium, resulting in the faint extended parts. Therefore, the mock observation with the different thresholds of surface brightness can miss the both excitation and recombination Ly $\alpha$  photons at the faint parts.

### 3.4. The Ly $\alpha$ Line Profile

The resulting Ly $\alpha$  line profiles of the modeled MW galaxy from  $z \sim 14$  to  $z \sim 6$  are shown in Figure 7. We randomly sample the frequency of the intrinsic Ly $\alpha$  photon from a Maxwellian distribution with the gas temperature at the emission location. All sources show asymmetric profiles with a single peak or weak double peaks. More interestingly, most profiles are shifted to the shorter (bluer) wavelengths. This is a characteristic feature of gas inflow (Zheng & Miralda-Escudé 2002). Indeed, as shown in Figure 8, a significant fraction of the gas shows a large infalling velocity  $V_r \sim -100$  to  $\sim -200$  km s $^{-1}$ , even though our simulation includes feedback of stellar wind similar to that of Springel et al. (2005). In particular, the gas in the galaxy from  $z \sim 14$ –10 is dominated by inflow motion, which explains the significant blue shift of the profiles in Figure 7 (top panel). At redshift  $z \lesssim 8.5$ , the gas exhibits outflow as well, and has a larger velocity distribution  $-250 \lesssim V_r \lesssim 200$  km s $^{-1}$ , which results in an extended profile to both blue and red wings. While asymmetric line profiles with an extended red wing are commonly seen in high-redshift LAEs, there appears to be some profiles in the  $z \gtrsim 6$  observations that have complex features including double peaks and extended blue wing, similar to what we see here (e.g., Ouchi et al. 2010; Hu et al. 2010; Kashikawa et al. 2011). The observed line of z8\_GND\_5296, the most distant LAE at  $z = 7.5$ , is not resolved well and thus has a Gaussian

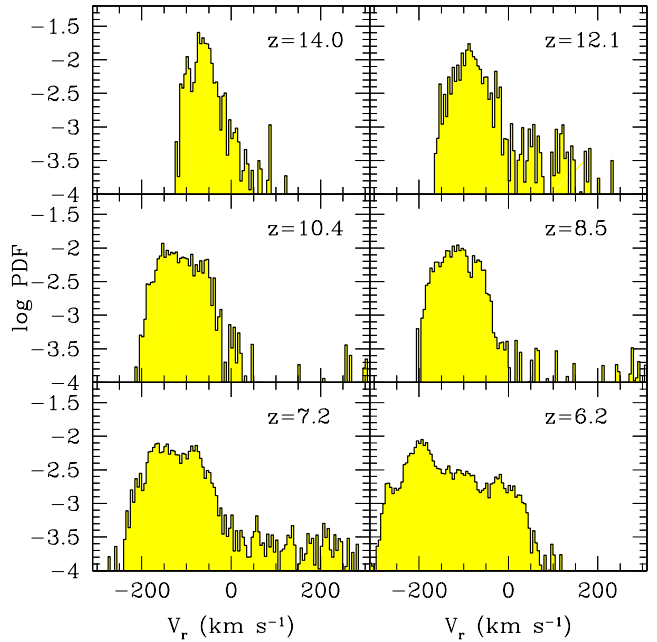


**Figure 8.** The probability distribution function of the gas mass of the neutral hydrogen in the galaxy as a function of radial velocity. The velocity is estimated from the center of mass of the galaxy in the radial direction.

profile (Finkelstein et al. 2013). More observations of high-resolution Ly $\alpha$  line profiles of high-redshift LAEs are needed to test our model and verify our predictions.

We note that the Ly $\alpha$  line profile may be suppressed and changed by the intergalactic medium (IGM) (e.g., Santos 2004; Dijkstra et al. 2007; Zheng et al. 2010; Laursen et al. 2011), because the IGM effectively scatters the Ly $\alpha$  photons at the line center and at shorter wavelengths by the Hubble flow (e.g., Laursen et al. 2011). As a result, the inflow feature in our profiles may disappear and the shape may become an asymmetric single peak with only photons at red wing. Laursen et al. (2011) showed that a large fraction of Ly $\alpha$  flux from galaxies at  $z \sim 6.5$  could be lost by scattering in IGM despite most of IGM were ionized. As a simple test, we show the line profiles without photons at the shorter wavelength as shown in the blue dash lines in the figure. As a result, about 0.59 (0.54) of Ly $\alpha$  flux from the galaxies at  $z = 12.1$  (6.2) are lost. The inflow feature completely disappears, and the asymmetric profiles with the red wings may be recognized as the galaxies have gas outflow. In addition, if IGM is highly neutral, even Ly $\alpha$  flux at red wing is highly suppressed. For neutral IGM, the IGM optical depth is estimated by  $\tau(\Delta v) \sim 2.3 \left( \frac{\Delta v}{600 \text{ km/s}} \right) \left( \frac{1+z}{10} \right)^{3/2}$  (Dijkstra & Wyithe 2010), where  $\Delta v$  is the velocity shift from the line center. More than 0.99 of Ly $\alpha$  fluxes from our model galaxies are lost for the neutral IGM. Therefore, if IGM is highly neutral, Ly $\alpha$  flux from our model galaxies cannot be observed.

### 3.5. Detectability of Progenitors of Local $L^*$ Galaxies

The emergent multi-wavelength SEDs of the MW galaxy at different redshifts are shown in Figure 9. The

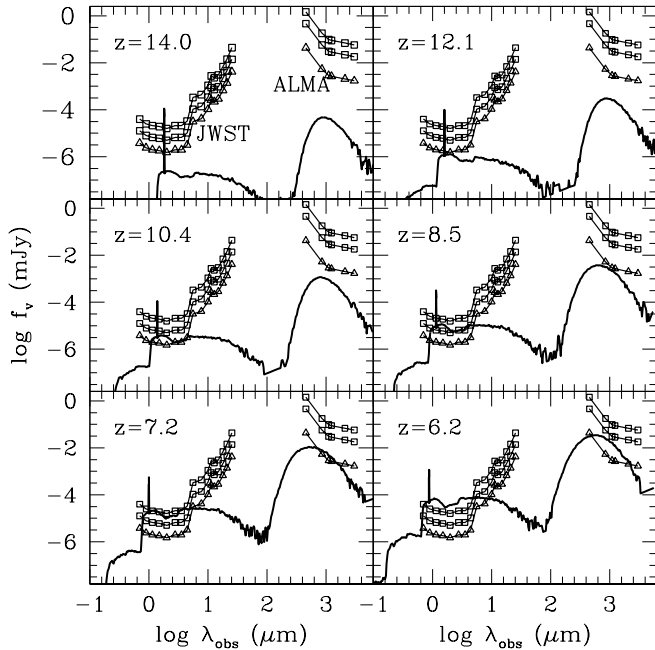


**Figure 9.** The spectral energy distribution of the MW galaxy at different redshift and its detectability with JWST and ALMA. The open squares indicate the  $10\sigma$  detection limits of JWST and ALMA with 16 antennas at an integration time of 1 and 10 hours (from top to bottom), while the open triangles indicate the  $3\sigma$  detection limits of JWST and ALMA with 50 antennas.

shape of the SEDs evolves with redshift due to the change of intrinsic stellar radiation, absorption of continuum photons by gas and dust, and thermal emission by dust. In all cases, the strong Ly $\alpha$  lines emerge, and at  $z \gtrsim 8.5$  the UV continuum at  $\lambda \leq 912 \text{ \AA}$  in rest frame is deeply declined due to strong absorption because of dense neutral hydrogen gas around star forming region.

A major science goal of the two forthcoming telescopes, ALMA and JWST, is to detect the first galaxies. In order to predict the detectability of the infancy of a local  $L^*$  galaxy, we contrast the SEDs with some detection limits of these two facilities in Figure 9. Our calculations show that the flux at  $850 \mu\text{m}$  in the observed frame of the model galaxy ranges from  $\sim 7.9 \times 10^{-5} \text{ mJy}$  at  $z = 14.0$  to  $\sim 4.7 \times 10^{-2} \text{ mJy}$  at  $z = 6.2$ . With an array of 50 antennas and an integration of 10 hours, ALMA may be able to detect such galaxies at  $z \lesssim 8.5$  with a  $3\sigma$  significance. However, since galaxies do not have a lot of young stars and much dust at  $z \gtrsim 10$ , observations in continuum by ALMA becomes more difficult, and it would need tens of hours of integration time. In contrast, JWST appears to be more powerful to detect the earliest galaxies as the one we model here, because it can detect the UV continuum in rest frame up to  $z \sim 10$ . The Ly $\alpha$  emission is strong even at  $z \sim 12$ , which may be observable by Near-Infrared Spectrograph (NIRSpec) on JWST. The NIRSpec will have the detection threshold of  $\sim 3 \times 10^{-18} \text{ erg s}^{-1} \text{ cm}^{-2}$  with  $R = 100$  and S/N = 10 by exposure time of  $10^4$  seconds.

We note that in the above estimation, IGM absorption and transmission were not taken into account. The IGM can significantly suppress the Ly $\alpha$  flux, and

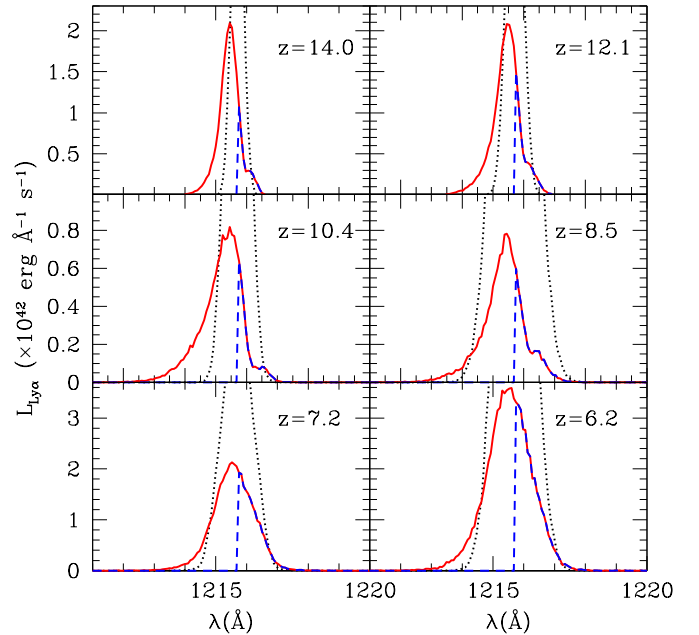


**Figure 10.** Same as in Figure 7, but here the simulation does not include the wind model from stellar feedback.

the transmission highly depends on viewing angle (e.g., Laursen et al. 2011) by inhomogeneous ionization structure in IGM (e.g., Abel et al. 2007; Yoshida et al. 2007; Jeon-Daniel et al. 2012), which make the detection more difficult. Of course, the galaxies we present here represent progenitor of a local  $L^*$  galaxy such as the Milky Way. Galaxies formed in highly overdense regions are likely much more massive (Li et al. 2007), and may be more easily detected by both ALMA and JWST (Li et al, in preparation).

#### 4. DISCUSSIONS

The gas inflow feature is present in our simulation with outflow from stellar feedback. In order to probe the effect of stellar wind on the gas inflow, we also performed the simulation with a pure thermal feedback model, in which the feedback from supernovae is only in thermal energy. In such a model, some fraction of thermal energy can quickly escape as cooling radiation before conversion to kinetic energy. As a result, gas outflow does not occur efficiently.

The resulting Ly $\alpha$  line profiles and the probability distribution function of the neutral gas mass are shown in Figure 10 and Figure 11, respectively. Without a strong outflow, the Ly $\alpha$  line profiles show more pronounced blue wing. However, due to the IGM transmission, Ly $\alpha$  flux at the blue wing can be suppressed significantly. If Ly $\alpha$  photons at shorter wavelength than the line center are suppressed, 0.69 (0.44) of Ly $\alpha$  flux from the galaxies at  $z = 12.1$  (6.3) is lost (see the blue dash lines in Figure 10).

The galaxy in our simulation resides in a low overdensity region and it represents those that would evolve into present-day  $L^*$  galaxies such as the Milky Way, so it may not be the very first one formed in the universe. It is believed that the most massive halos in the highly overdense regions collapse first, in which the first stars form (e.g., Abel et al. 2002; Bromm & Larson 2004; Gao et al.



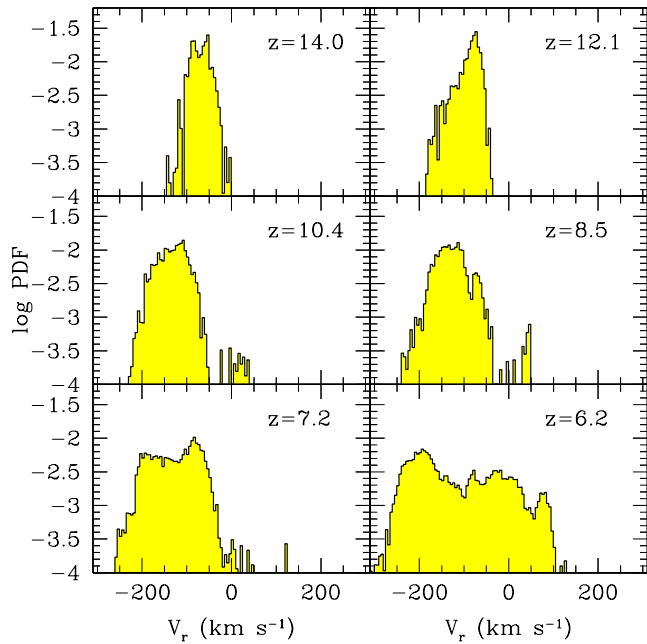


**Figure 11.** Same as Figure 8, but here the simulation does not include the wind model from stellar feedback. The probability distribution function of the gas mass of the neutral hydrogen in the galaxy as a function of radial velocity. The velocity is estimated from the center of mass of the galaxy in the radial direction.

2007; Yoshida et al. 2008). These may also be the formation sites of the very first galaxies, owing to feedback and chemical enrichment from the PopIII stars, as well as abundant gas supply (Li et al. 2007; Bromm et al. 2009).

One of the major limitations of our model is that the cosmological simulation does not have sufficient resolutions to follow the formation and evolution of individual stars. Instead, star formation is modeled using a “sub-grid” recipe based on the observed Schmidt-Kennicutt Law (Kennicutt 1998). Gas particles are converted into stars once it is cooled below  $10^4$  K and the density is above a threshold (Springel & Hernquist 2003). Although this treatment is rather simplistic, it nevertheless gives a global star formation history close to what is believed of the MW galaxy.

Another major limitation is that our current RT calculations do not include the propagation and scattering of Ly $\alpha$  and ionizing photons in the IGM. We make the prediction that galaxies with inflow of cold gas would result in asymmetric, blue-shifted Ly $\alpha$  line profiles. However, as discussed earlier, the absorption by IGM may change the the profile to one with extended red wing. We will study this issue in more detail in future work that includes the radiative transfer of Ly $\alpha$  and ionizing photons in the IGM.

## 5. SUMMARY

In this work, we have investigated the formation of a typical, nearby  $L^*$  galaxy such as the MW, and its Ly $\alpha$  properties at the earliest evolutionary stage. We combine a cosmological hydrodynamic simulation, which uses the Aquila initial condition and focuses on a MW-like galaxy, with three-dimensional radiative transfer calculations using the improved ART<sup>2</sup> code, which couples

multi-wavelength continuum, Ly $\alpha$  line, and ionization of hydrogen.

We find that the modeled MW galaxy forms from efficient accretion of cold gas early on, which sustains a high star formation rate from  $z \sim 14 - 6$ . The cold accretion produces strong Ly $\alpha$  emission via collisional excitation, which has a luminosity from  $\sim 1.6 \times 10^{42}$  erg s<sup>-1</sup> at  $z \sim 14$  to  $\sim 5.5 \times 10^{42}$  erg s<sup>-1</sup> at  $z \sim 6$ . The escape fraction of Ly $\alpha$  photons increases from  $\sim 0.49$  at  $z \sim 6$  to  $\sim 0.81$  at  $z \sim 14$ , due to less dust content at higher redshift. The EWs of the Ly $\alpha$  lines increases with redshift, from  $\sim 93$  Å at  $z \sim 6$  to  $\sim 2300$  Å at  $z \sim 14$ . Such high EWs may be due to significant contribution to Ly $\alpha$  emission by excitation cooling, which dominates at high redshift. The resulting Ly $\alpha$  lines exhibit asymmetric, mostly single-peak profiles shifted to the blue wing, a characteristic feature of inflow.

Furthermore, we demonstrate that progenitors of local  $L^*$  galaxies such as the modeled one may be detected at  $z \lesssim 8$  by JWST and ALMA with a reasonable integration time. At higher redshift  $z \gtrsim 12$ , however, only Ly $\alpha$  line may be observable by spectroscopic surveys with similar detection limit as JWST.

Our results suggest that Ly $\alpha$  line may be used to probe the formation and evolution, and gas properties of distant galaxies. It is perhaps one of the most powerful tools to detect the first generation of galaxies in the coming decade.

We thank Carlos Frenk for kindly providing the Aquila initial conditions to us, and Masayuki Umemura for stimulating discussions and helpful comments. We also thank the anonymous referee for useful comments. HY is grateful to Takatoshi Shibuya, Alex Hagan, and Robin Ciardullo for valuable discussion about the sensitivity of JWST. This research is supported by NSF grants AST-0965694, AST-1009867, and AST-0807075. We thank the Research Computing and Cyberinfrastructure (unit of Information Technology Services) at the Pennsylvania State University for providing computational resources and services. The Institute for Gravitation and the Cosmos (IGC) is supported by the Office of the Senior Vice President for Research and the Eberly College of Science at the Pennsylvania State University.

## REFERENCES

- Abel, T., Bryan, G. L., & Norman, M. L. 2002, *Science*, 295, 93  
 Abel, T., Wise, J. H., & Bryan, G. L. 2007, *ApJ*, 659, L87  
 Beichman, C. A. and Rieke, M. and Eisenstein, D., et al. 2012, *Proceedings of the SPIE, Space Telescopes and Instrumentation 2012: Optical, Infrared, and Millimeter Wave.*, Volume 8442  
 Birnboim, Y. & Dekel, A. 2003, *MNRAS*, 345, 349  
 Bouwens, R. J. & Illingworth, G. D. 2006, *Nature*, 443, 189  
 Bouwens, R. J., Illingworth, G. D., Labbe, I., et al. 2011, *Nature*, 469, 504  
 Bouwens, R. J., Illingworth, G. D., Oesch, P. A., et al. 2010, *ApJ*, 709, L133  
 Bouwens, R. J., Thompson, R. I., Illingworth, G. D., et al. 2004, *ApJ*, 616, L79  
 Bromm, V. & Larson, R. B. 2004, *ARA&A*, 42, 79  
 Bromm, V. & Yoshida, N. 2011, *ARA&A*, 49, 373  
 Bromm, V., Yoshida, N., Hernquist, L., & McKee, C. F. 2009, *Nature*, 459, 49  
 Brooks, A. M., Governato, F., Quinn, T., Brook, C. B., & Wadsley, J. 2009, *ApJ*, 694, 396

- Bruzual, G. & Charlot, S. 2003, MNRAS, 344, 1000
- Bryan G. L., Norman M. L., 1998, AJ, 495, 80
- Davé, R., Hernquist, L., Katz, N., & Weinberg, D. H. 1999, ApJ, 511, 521
- Dekel, A. & Birnboim, Y. 2006, MNRAS, 368, 2
- Dekel, A., Birnboim, Y., Engel, G., et al. 2009, Nature, 457, 451
- Di Matteo, T., Khandai, N., DeGraf, C., et al. 2012, ApJ, 745, L29
- Dijkstra, M., Lidz, A., & Wyithe, J. S. B. 2007, MNRAS, 377, 1175
- Dijkstra, M. & Loeb, A. 2009, MNRAS, 400, 1109
- Dijkstra, M. & Wyithe, J. S. B. 2010, MNRAS, 408, 352
- Faucher-Giguère, C., Kereš, D., Dijkstra, M., Hernquist, L., & Zaldarriaga, M. 2010, ApJ, 725, 633
- Faucher-Giguère, C., Lidz, A., Zaldarriaga, M., & Hernquist, L. 2009, ApJ, 703, 1416
- Finkelstein, S. L., Papovich, C., Dickinson, M., et al. 2013, Nature, 502, 524
- Gao, L., Yoshida, N., Abel, T., et al. 2007, MNRAS, 378, 449
- Goerdt, T., Dekel, A., Sternberg, A., et al. 2010, MNRAS, 407, 613
- Greif, T. H., Glover, S. C. O., Bromm, V., & Klessen, R. S. 2010, ApJ, 716, 510
- Gronwall, C., Ciardullo, R., Hickey, T., et al. 2007, ApJ, 667, 79
- Haardt, F. & Madau, P. 1996, ApJ, 461, 20
- Hernquist, L. & Katz, N. 1989, ApJS, 70, 419
- Hasegawa, K., & Semelin, B. 2013, MNRAS, 428, 154
- Hu, E. M., Cowie, L. L., Barger, A. J., et al. 2010, ApJ, 725, 394
- Hui, L. & Gnedin, N. Y. 1997, MNRAS, 292, 27
- Iye, M., Ota, K., Kashikawa, N., et al. 2006, Nature, 443, 186
- Jeeson-Daniel, A., Ciardi, B., Maio, U., et al. 2012, MNRAS, 424, 2193
- Jeon, M., Pawlik, A. H., Greif, T. H., et al. 2012, ApJ, 754, 34
- Kashikawa, N., Shimasaku, K., Matsuda, Y., et al. 2011, ApJ, 734, 119
- Katz, N., Keres, D., Dave, R., & Weinberg, D. H. 2003, in Astrophysics and Space Science Library, Vol. 281, The IGM/Galaxy Connection. The Distribution of Baryons at  $z=0$ , ed. J. L. Rosenberg & M. E. Putman, 185–+
- Katz, N., Weinberg, D. H., Hernquist, L., & Miralda-Escude, J. 1996, ApJ, 457, L57+
- Kennicutt, Jr., R. C. 1998, ARA&A, 36, 189
- Kereš, D., Katz, N., Fardal, M., Davé, R., & Weinberg, D. H. 2009, MNRAS, 395, 160
- Kereš, D., Katz, N., Weinberg, D. H., & Davé, R. 2005, MNRAS, 363, 2
- Komatsu, E., Dunkley, J., Nolta, M. R., et al. 2009, ApJS, 180, 330
- Latif, M. A., Zaroubi, S., & Spaans, M. 2011, MNRAS, 411, 1659
- Laursen, P., Sommer-Larsen, J., & Razoumov, A. O. 2011, ApJ, 728, 52
- Lehnert, M. D., Nesvadba, N. P. H., Cuby, J., et al. 2010, Nature, 467, 940
- Li, Y., Hernquist, L., Robertson, B., et al. 2007, ApJ, 665, 187
- Li, Y., Hopkins, P. F., Hernquist, L., et al. 2008, ApJ, 678, 41
- Malhotra, S. & Rhoads, J. E. 2004, ApJ, 617, L5
- Matsuda, Y., Yamada, T., Hayashino, T., et al. 2012, MNRAS, 425, 878
- Ocvirk, P., Pichon, C., & Teyssier, R. 2008, MNRAS, 390, 1326
- Ono, Y., Ouchi, M., Mobasher, B., et al. 2012, ApJ, 744, 83
- Osterbrock, D. E. & Ferland, G. J. 2006, Astrophysics of gaseous nebulae and active galactic nuclei, ed. Osterbrock, D. E. & Ferland, G. J., Astrophysics of gaseous nebulae and active galactic nuclei
- Ouchi, M., Shimasaku, K., Akiyama, M., et al. 2008, ApJS, 176, 301
- Ouchi, M., Shimasaku, K., Furusawa, H., et al. 2010, ApJ, 723, 869
- Rosdahl, J., & Blaizot, J. 2012, MNRAS, 423, 344
- Salpeter, E. E. 1955, ApJ, 121, 161
- Santos, M. R. 2004, MNRAS, 349, 1137
- Scannapieco, C., Wadepuhl, M., Parry, O. H., et al. 2012, MNRAS, 423, 1726
- Schmidt, M. 1959, ApJ, 129, 243
- Shibuya, T., Kashikawa, N., Ota, K., et al. 2012, ApJ, 752, 114
- Springel, V. 2005, MNRAS, 364, 1105
- Springel, V., Di Matteo, T., & Hernquist, L. 2005, MNRAS, 361, 776
- Springel, V. & Hernquist, L. 2002, MNRAS, 333, 649
- . 2003, MNRAS, 339, 289
- Springel, V., Wang, J., Vogelsberger, M., et al. 2008, MNRAS, 391, 1685
- Springel, V., Yoshida, N., & White, S. D. M. 2001, New Astronomy, 6, 79
- Stark, D. P., Ellis, R. S., & Ouchi, M. 2011, ApJ, 728, L2
- Stark, D. P., Ellis, R. S., Richard, J., et al. 2007, ApJ, 663, 10
- Thoul, A. A., & Weinberg, D. H. 1996, ApJ, 465, 608
- Vanzella, E., Pentericci, L., Fontana, A., et al. 2011, ApJ, 730, L35
- Wadepuhl, M. & Springel, V. 2011, MNRAS, 410, 1975
- Wise, J. H. & Abel, T. 2007, ApJ, 665, 899
- . 2008, ApJ, 685, 40
- Wise, J. H., Turk, M. J., & Abel, T. 2008, ApJ, 682, 745
- Wise, J. H., Turk, M. J., Norman, M. L., & Abel, T. 2012, ApJ, 745, 50
- Yajima, H., Li, Y., Zhu, Q., & Abel, T. 2012a, MNRAS, 424, 884
- Yajima, H., Li, Y., Zhu, Q., et al. 2012b, ApJ, 754, 118
- Yajima, H., Li, Y., Zhu, Q., et al. 2012c, submitted to MNRAS, arXiv: 1209.5842
- Yoshida, N., Oh, S. P., Kitayama, T., & Hernquist, L. 2007, ApJ, 663, 687
- Yoshida, N., Omukai, K., & Hernquist, L. 2008, Science, 321, 669
- Zheng, Z., Cen, R., Trac, H., & Miralda-Escudé, J. 2010, ApJ, 716, 574
- Zheng, Z. & Miralda-Escudé, J. 2002, ApJ, 578, 33
- Zhu, Q. and Li, Y. and Sherman, S. 2012, submitted to ApJ, arXiv: 1211.0013